communications materials

Article

https://doi.org/10.1038/s43246-024-00666-2

Microscopic probing of the superconducting and normal state properties of $Ta_2V_{3.1}Si_{0.9}$ by muon spin rotation

J. N. Graham[1], H. Liu[2,3], V. Sazgari[1], C. Mielke III[1], M. Medarde[1], H. Luetkens[1], R. Khasanov[1], Y. Shi[2,3,4] & Z. Guguchia[1]

The two-dimensional kagome lattice is an experimental playground for novel physical phenomena, from frustrated magnetism and topological matter to chiral charge order and unconventional superconductivity. A newly identified kagome superconductor, $Ta_2V_{3.1}Si_{0.9}$ has recently gained attention for possessing a record high critical temperature, T_C = 7.5 K for kagome metals at ambient pressure. In this study we conducted a series of muon spin rotation measurements to delve deeper into understanding the superconducting and normal state properties of $Ta_2V_{3.1}Si_{0.9}$. We demonstrate that $Ta_2V_{3.1}Si_{0.9}$ is a bulk superconductor with either a s+s-wave or anisotropic s-wave gap symmetry, and has an unusual paramagnetic shift in response to external magnetic fields in the superconducting state. Additionally, we observe an exceptionally low superfluid density – a distinctive characteristic of unconventional superconductivity – which remarkably is comparable to the superfluid density found in hole-doped cuprates. In its normal state, $Ta_2V_{3.1}Si_{0.9}$ exhibits a significant increase in the zero-field muon spin depolarisation rate, starting at approximately 150 K, which has been observed in other kagome-lattice superconductors, and therefore hints at possible hidden magnetism. These findings characterise $Ta_2V_{3.1}Si_{0.9}$ as an unconventional superconductor and a noteworthy new member of the vanadium-based kagome material family.

As a result of the complex interactions between a materials chemical structure and electronic properties, superconductivity in materials with exotic lattice geometries has emerged as a frontier in condensed matter physics. Among these, the kagome lattice stands out due to its distinctive two-dimensional lattice comprised of corner-sharing triangles[1–4], which gives rise to a number of fascinating electronic phenomena such as flat bands[2, 5], Van Hove singularities[6–8] and Dirac cones[5,9]. These features are critical as they can significantly alter the density of states at the Fermi level, potentially leading to high-temperature superconductivity and other novel ground states.

Some of the most extensively studied kagome superconductors are the AV_3Sb_5 family[10–12], which are renowned for their unconventional superconducting characteristics, from transitions from nodal to nodeless pairing[13], to pronounced pressure effects on superfluid density[14–16], and time-reversal symmetry (TRS) breaking states associated with charge ordering[17–19]. These phenomena highlight the complex interplay between the lattice geometry and electronic properties that are unique to kagome superconductors.

Another notable compound in this context is $LaRu_3Si_2$, which not only exhibits a relatively high critical temperature of T_c = 6.5 K but also shows indications of unconventional superconductivity[20–26]. Recent studies have uncovered distinct charge orders in $LaRu_3Si_2$[26], with one such order appearing above room temperature and a second one which breaks TRS, further underscoring the potential for exotic ground states in kagome lattice structures to emerge. These findings show that the kagome lattice can host a range of novel electronic phenomena, stemming from the complex interplay between intrinsic geometric frustration, electron correlations and electron-phonon coupling.

[1]PSI Center for Neutron and Muon Sciences CNM, 5232 Villigen PSI, Switzerland. [2]Beijing National Laboratory for Condensed Matter Physics, Institute of Physics, Chinese Academy of Sciences, Beijing, 100190, China. [3]School of Physical Sciences, University of Chinese Academy of Sciences, Beijing, 100190, China. [4]Songshan Lake Materials Laboratory, Dongguan, Guangdong, 523808, China. e-mail: zurab.guguchia@psi.ch

Recently, a new kagome superconductor, $Ta_2V_{3.1}Si_{0.9}$, was reported, boasting the highest known T_c of 7.5 K among kagome superconductors at ambient pressure[27]. Whilst initial reports have primarily documented the basic characteristics of its superconductivity, there remains a vast, largely untapped potential to explore its microscopic properties both in the superconducting and normal states. The high T_c and the unexplored nature of $Ta_2V_{3.1}Si_{0.9}$ make it a prime candidate for investigating the unconventional aspects of superconductivity and the possibility of TRS-breaking phenomena in its normal state properties. This study aims to delve deeper into these aspects by measuring the temperature and field dependence of the magnetic penetration depth and TRS breaking response using the technique of muon-spin rotation. This work contributes to the broader understanding of how kagome superconductors can challenge and expand our current knowledge of superconducting mechanisms and electronic order.

Results

Polycrystalline samples of $Ta_2V_{3.1}Si_{0.9}$ were synthesised according to other reports[27]. $Ta_2V_{3.1}Si_{0.9}$ adopts the hexagonal $P6_3/mmc$ structure in which staggered vanadium kagome layers and Ta_2Si are alternately stacked along the c-axis (Fig. 1a)[27]. Though the kagome sublattice is nearly structurally perfect, with only a slight difference in bond lengths (Fig. 1b), the extra V ions randomly occupy the 2a site which is nominally occupied fully by Si. A full discussion of the structural properties of $Ta_2V_{3.1}Si_{0.9}$ can be found in Ref. 27.

Figure 1c shows the temperature dependence of the field cooled (FC) and zero field cooled (ZFC) magnetic susceptibility, $\chi(T)$ in an applied magnetic field of 2 mT. A large diamagnetic signal and splitting between the FC and ZFC curves indicates the onset of bulk superconductivity in $Ta_2V_{3.1}Si_{0.9}$ with a critical temperature, $T_c \simeq 7.8$ K. The superconducting shielding fraction can be estimated to be ~50%. The susceptibility was also measured over a larger temperature range in a 3 mT applied field (Fig. 1d) where we observe two weak divergences between the ZFC and FC data, firstly at ~300K, which is potentially due to a small impurity in the sample[27], and then a larger divergence at $T^* \sim 150$K. One plausible explanation to the T^* transition could be that the magnetic structure of $Ta_2V_{3.1}Si_{0.9}$ is comprised of different ferromagnetic domains which are randomly orientated with respect to each other. When low fields, such as 3 mT, are applied, the field is insufficient to align the magnetic moments. Further measurements in higher fields show a gradual closing of the gap, and by 1 T the gap is completely closed, suggesting the domains are fully aligned.

Figure 2 a shows the transverse-field (TF)-μSR spectra for $Ta_2V_{3.1}Si_{0.9}$ measured in an applied magnetic field of 30 mT, above (10K, black) and below (0.27K, green) the superconducting transition temperature, T_C. The data were collected after field-cooling the sample from above T_C. The applied field was selected based on the criterion $H_{c1} < H_{app} \ll H_{c2}$. Under this condition, a well-ordered Abrikosov vortex lattice is formed. Above T_C, the oscillations have a small relaxation due to the random local fields produced by the nuclear moments. Further damping of these oscillations are expected below T_C due to the presence of a non-uniform local field distribution produced by the formation of the flux-line lattice (FLL) in the superconducting state. The amount of damping is proportional to the inverse square of the London penetration depth. In the present system, $Ta_2V_{3.1}Si_{0.9}$, the damping exhibits only a very weak enhancement in the superconducting state. Under ZFC conditions, however, a strong damping of the asymmetry signal is observed. From this, we are able to draw three important conclusions: (1) The penetration depth is long, resulting in minimal damping produced by the well-ordered FLL from the FC conditions. (2) The vortices are strongly pinned, and therefore when the sample is cooled under ZFC conditions, a disordered vortex lattice is created, leading to artificially enhanced damping. (3) The strong damping observed under ZFC conditions indicates that $Ta_2V_{3.1}Si_{0.9}$ experiences bulk superconductivity. As shown by the solid lines in Fig. 2a, TF-μSR data were analysed using the following function[28]:

$$A_{TF}(t) = \sum_i^n A_{S,i} e^{\left[-\frac{(\sigma_{tot,i}t)^2}{2}\right]} \cos(\gamma_\mu B_{int,i} t + \phi_i) \quad (1)$$

where A_S describes the initial asymmetry, $\sigma_{tot}(=\sqrt{\sigma_{sc}^2+\sigma_{nm}^2})$ is the total muon depolarisation rate, which is comprised of superconducting, σ_{sc} and nuclear magnetic dipolar, σ_{nm} contributions, $\gamma_\mu/(2\pi) \simeq 135.5$ MHz/T is the

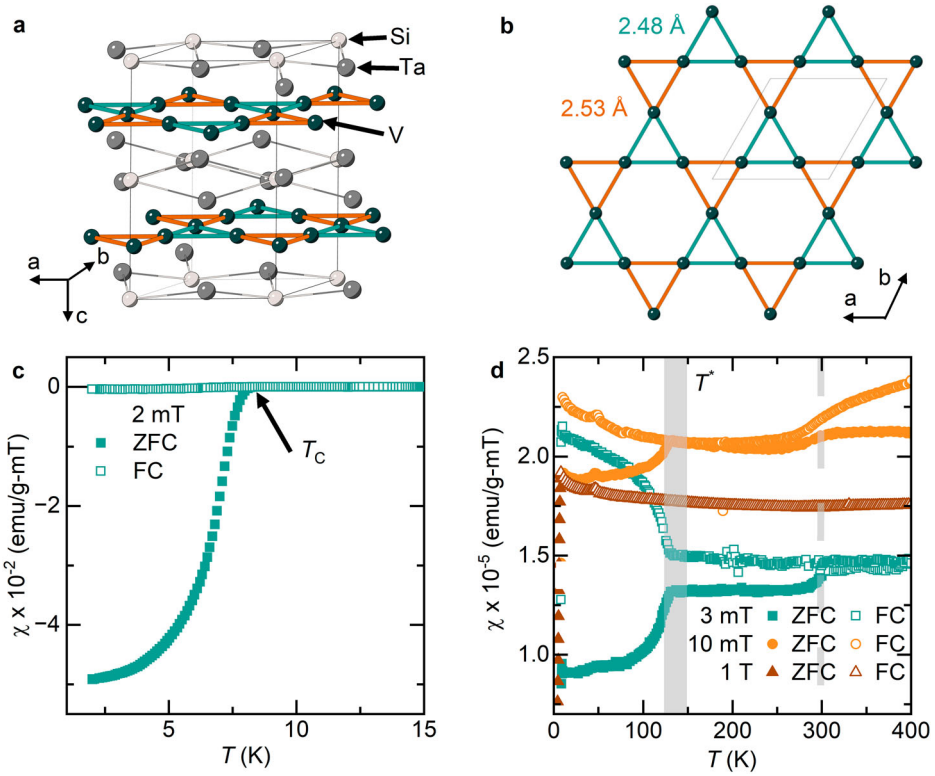

Fig. 1 | Crystal structure and magnetic susceptibility data of $Ta_2V_{3.1}Si_{0.9}$. a $Ta_2V_{3.1}Si_{0.9}$ adopts the $P6_3/mmc$ crystal structure in which staggered vanadium kagome networks are stacked between layers of Ta_2Si along the c-axis. **b** The kagome lattice of $Ta_2V_{3.1}Si_{0.9}$ is constructed from two slightly different sized triangles, with bond lengths 2.48 Å; (green) and 2.53 Å; (orange). **c** ZFC magnetic susceptibility data measured in an applied field of 2 mT show a sharp drop at $T_C = 7.8$K. **d** High-temperature magnetic susceptibility measured at 3 mT, where a clear divergence between the FC and ZFC data occurs, first at $T \sim 300$K and then again at $T^* = 150$K. Further data measured at 10 mT and 1 T are also shown. The error bars are smaller than the size of the symbols.

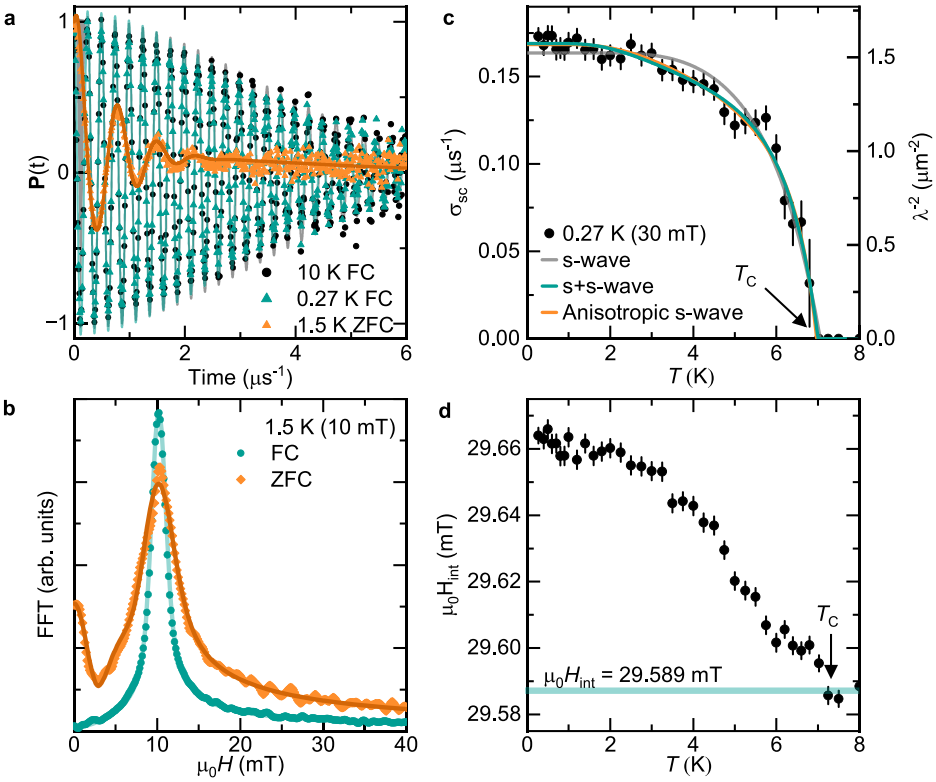

Fig. 2 | Summary of μSR experiments in the superconducting state of $Ta_2V_{3.1}Si_{0.9}$. **a** Transverse-field (TF) μSR spectra collected above (10 K, black) and below (0.27K, green) T_C after field-cooling the sample from above T_C in a 30 mT applied magnetic field, and data recorded at 1.5K (10 mT, orange) from a zero-field-cooling cycle. The spectra are presented in terms of the polarisation, $P(t) = A_{TF}/A_0$. Error bars are the standard error on the mean (s.e.m) of about 10^6 events. The error of each bin count, n is given by the standard deviation (s.d.) of n. The errors of each bin in $P(t)$ are then calculated by standard-error propagation. **b** Fourier transforms of data collected at 1.5K in FC (green) and ZFC (orange) cycles. **c** Temperature dependence of the superconducting muon depolarisation rate, σ_{sc} and inverse squared penetration depth, λ^{-2} measured in 30 mT. Different models for the superconducting gap symmetry are included, with the $s + s$-wave and anisotropic s-wave being indistinguishable. The error arising from the nuclear contribution is assumed to be zero. **d** Temperature dependence of the internal magnetic field, $\mu_0 H_{int}$ measured in the superconducting state. The error bars represent the standard deviation of the fit parameters.

gyromagnetic ratio of the muon, B_{int} is the internal magnetic field, and ϕ is the initial phase of the muon ensemble. Since the Fourier transform (FT) of the FC spectrum is sharp and symmetrical (Fig. 2b), only one component is required in the fit, whereas for the ZFC case, three broad components were fit to the data. All three components are displaced from the applied field, with two of them being shifted significantly farther away. These two components can be attributed as originating fully from the superconducting part of the sample. While the narrowest peak, located at the applied field, may represent the background and the non-superconducting part of the signal. From this we are able to estimate that at least 81% of the sample is superconducting. All subsequent analysis will be conducted on the FC data.

Figure 2c shows σ_{sc} as a function of temperature for $Ta_2V_{3.1}Si_{0.9}$ measured under an applied field of 30 mT. During the analysis, σ_{nm} was assumed to be constant over the whole measured temperature range, and since in the normal state σ_{nm} is the only contributor to the depolarisation rate, an average of σ_{tot} was taken above T_C and subtracted in quadrature from σ_{tot} to leave just the superconducting fraction, σ_{sc}. Below T_C, the depolarisation rate increases from zero due to the formation of the FLL, and saturates at the lowest temperatures. The very dilute superfluid density appears to be correlated to a relatively high T_C, and this is an experimental indicator of unconventional superconductivity. It is also important to note at this point that below T_C, we observe an anomalous paramgnetic shift of the internal magnetic field, B_{int}, as oppose to the expected diamagnetic shift of a superconductor (Fig. 2d).

To explore the superconducting gap symmetry of $Ta_2V_{3.1}Si_{0.9}$, we performed a quantitative analysis by first relating the muon spin depolarisation rate, $\sigma_{sc}(T)$ in the presence of a perfect triangular vortex lattice to the London penetration depth, $\lambda(T)$ by the following equation[29,30]:

$$\frac{\sigma_{sc}(T)}{\gamma_\mu} = 0.06091\frac{\Phi_0}{\lambda^2(T)} \quad (2)$$

where $\Phi_0 = 2.068 \times 10^{15}$Wb is the magnetic flux quantum. This equation is valid since $H_{app} \ll H_{c2}$, as $\mu_0 H_{c2}$ was previously determined to be 14.2T[27]. In this condition, according to the London model, σ_{sc} is field independent[29]. By evaluating the T dependence, which is directly associated with the superconducting gap, $\lambda(T)$ can be described within the local (London) approximation ($\lambda \gg \xi$) with the following[28]:

$$\frac{\lambda^{-2}(T,\Delta_{0,i})}{\lambda^{-2}(0,\Delta_{0,i})} = 1 + \frac{1}{\pi}\int_0^{2\pi}\int_{\Delta(T,\phi)}^{\infty}\left(\frac{\delta f}{\delta E}\right)\frac{EdEd\varphi}{\sqrt{E^2-\Delta_i(T,\varphi)^2}} \quad (3)$$

where $f = [1 + \exp(E/k_BT)]^{-1}$ is the Fermi function, φ is the angle along the Fermi surface, and $\Delta_i(T,\varphi) = \Delta_{0,i}\Gamma(T/T_C)g(\varphi)$ ($\Delta_{0,i}$ is the maximum gap value at $T = 0$). The temperature dependence of the gap is approximated by the expression, $\Gamma(T/T_C = \tanh 1.82[1.018(T_C/T-1)]^{0.51}$[31], whilst $g(\varphi)$ describes the angular dependence of the new gap and is replaced by 1 for an s-wave gap, $[1 + a\cos(4\varphi)/(1 + a)]$ for an anisotropic s-wave gap, and $|\cos(2\varphi)|$ for a d-wave gap[32].

The fits of different superconducting gap models are shown in Fig. 2c, with our analysis being unable to distinguish between a $s + s$-wave (green) and anisotropic s-wave (orange) model. A summary of the key parameters can be found in Table 1. Previous analysis of specific heat capacity data showed a plateauing of ΔC below 3K[27] which is characteristic of s-wave symmetry. However, a single s-wave model (grey line) does not capture the shape of σ_{sc}, and had significantly higher goodness of fit parameters than the other models tried in this work. We then tried more complex models, including $s + s$, anisotropic s and $s + d$. All gave qualitatively similar results, however the error on the "d" gap in the $s + d$ model was significant at 60%, and was therefore excluded from the analysis. From the fit, we were able to derive the London penetration depth, $\lambda(T > 0)$, which is relatively long at ~790 nm, and therefore explains the weak damping response of the μSR signal below T_C. In both cases, $T_C \approx 7$K, estimated from the superfluid density measurements, is concomitant with the value derived from previously reported magnetic susceptibility and resistivity measurements[27].

Moving on to the normal state properties, zero-field (ZF) and longitudinal-field (LF - field is applied parallel to the muon spin polarisation) measurements up to 20 mT, were collected at 10 K and are shown in

Fig. 3a. The ZF-μSR data were fit with a Gaussian Kubo-Toyabe depolarisation function, convoluted with an exponential term:

$$P_{ZF}^{GKT}(t) = \left(\frac{1}{3} + \frac{2}{3}(1-\Delta^2 t^2)\exp\left[-\frac{\Delta^2 t^2}{2}\right]\right)\exp(-\Gamma t) \quad (4)$$

where Δ/γ_μ is the width of the local field distribution primarily due to the nuclear moments but may also have some contribution from a dense network of weak electronic moments. The addition of the exponential Γ function is essential for modelling the data and may originate from static dilute electronic moments or dynamical fluctuations. The dynamic nature of Γ is evident from the LF measurements as under the application of a small magnetic field of 2.5 mT the relaxation is not fully decoupled and exhibits a purely exponential form. Upon increasing the magnetic field further, the relaxation is fully decoupled at 10 mT. This behaviour proves that the relaxation Δ is due to spontaneous fields that are static on the microsecond timescale, whereas the Γ rate is dynamic in origin. This doesn't imply that the fluctuations are confined to spatially separate regions; rather, they influence the entire sample uniformly. The exact origin of this dynamic signal is unclear and warrants further study.

Figure 3 b shows the evolution of the static, Δ and dynamic, Γ depolarisation rates in ZF over a wide temperature range. The magnitude of the Δ and Γ rates, particularly above T^*, are similar in magnitude and therefore are correlated. This is clearly illustrated by the small bump in Δ at 225K which is mirrored in Γ. This does not impact the main findings from this data, as the sizeable increase in Δ below $T^* \simeq 150$K indicates the ordering of the static moments, which in turn causes a slowing down of the dynamic (Γ) moments. This increase in Δ is reminiscent of other kagome superconductors, such as the AV_3Sb_5 compounds[12,33], in which increases in the muon depolarisation rate were found to be caused by TRS breaking charge order state. Further measurements under an applied magnetic field (Fig. 4) of 4T show an increase in Δ by 30 % below $T^* \simeq 150$K, while the feature around 225K gets nearly unchanged. We believe that these features are associated to the onset of a weak magnetic phases which co-exists alongside the superconducting state. Finally, the dynamic relaxation rate Γ shows a weak temperature dependence without significant features at ~150K. The evolution of Γ from the LF 5 mT measurements is shown in Fig. 3b, which is almost zero and temperature independent, and therefore reflects that the relaxation is nearly fully decoupled by 5 mT.

Table 1 | Summary of superconducting gap parameters from the three models shown in Fig. 2c

	s-wave	*s* + *s*-wave	Anisotropic *s*-wave
$\lambda^{-2}(T=0)$ (μm^{-2})	1.52 (1)	1.57 (2)	1.62 (2)
$\lambda(T>0)$ (nm)	811	798	785
ω	1	0.8 (1)	1
T_C (K)	7.06 (2)	7.01 (4)	6.97 (3)
Δ_1 (meV)	1.81 (4)	2.3 (3)	2.08 (9)
Δ_2 (meV)	–	0.8 (2)	–
a	–	–	0.64 (5)
χ^2	91.5	53.1	54.3
χ^2/NDF	2.69	1.66	1.64

λ is the London penetration depth, ω is the phase fraction, Δ is the size of the gap, a is the anisotropy, and χ^2 amd χ^2/NDF are goodness of fit parameters.

Discussion

Through our microscopic investigation into the superconducting and normal state properties of $Ta_2V_{3.1}Si_{0.9}$ we have uncovered four key findings:

(1) Nodeless $s + s$ or anisotropic s-wave superconductivity was determined through the analysis of μSR data. This form of nodeless superconductivity is akin to what has been observed in other kagome materials such as AsV_3Sb_5[13,34–36], $LaRu_3Si_2$[25] and $CeRu_2$[25,37]. Further studies are required to determine which is the true gap symmetry, with techniques such as ARPES being suitable once single-crystal samples of $Ta_2V_{3.1}Si_{0.9}$ are available.

(2) The exceptionally dilute superfluid density, coupled with high T_C, is a strong indicator of unconventional superconductivity. To put this in context with other superconductors, Fig. 5 shows a logarithmic plot of T_C against the effective penetration depth, λ_{eff}^2. For unconventional superconductors a T_C/λ_{eff}^2 of 0.1−20 is expected, with some examples of (K,Rb)

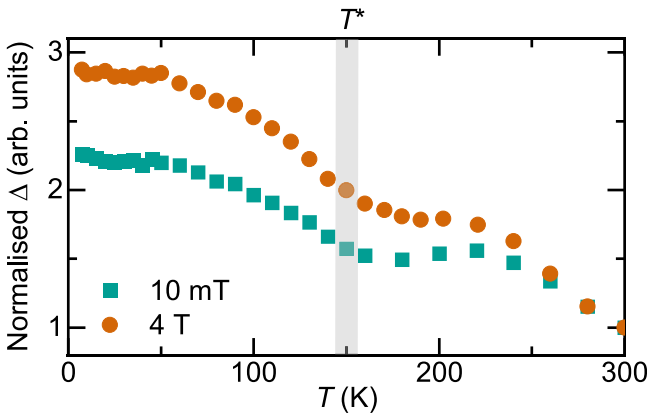

Fig. 4 | High field μSR results for $Ta_2V_{3.1}Si_{0.9}$. The temperature dependence of the muon spin relaxation rate, normalised to the value at 300 K, measured under the applied magnetic field of 10 mT and 4 T.

Fig. 3 | Summary of μSR experiments in the normal state of $Ta_2V_{3.1}Si_{0.9}$. a Zero-field (ZF) and longitudinal-field (LF) muon-spin rotation spectra, recorded at 10K in various applied fields up to 20 mT. Error bars are the standard error on the mean (s.e.m) of about 10^6 events. The error of each bin count, n is given by the standard deviation (s.d.) of n. The errors of each bin in $P(t)$ are then calculated by standard-error propagation. **b** Summary of muon-spin depolarisation rates, Δ (green square markers), and Γ (orange triangular markers) as a function of temperature. The temperature dependence of Γ measured under the applied magnetic field of 5 mT applied parallel to the muon spin polarisation is also shown. Inset shows the evolution of Γ as a function of the longitudinal field. The error bars represent the standard deviation of the fit parameters.

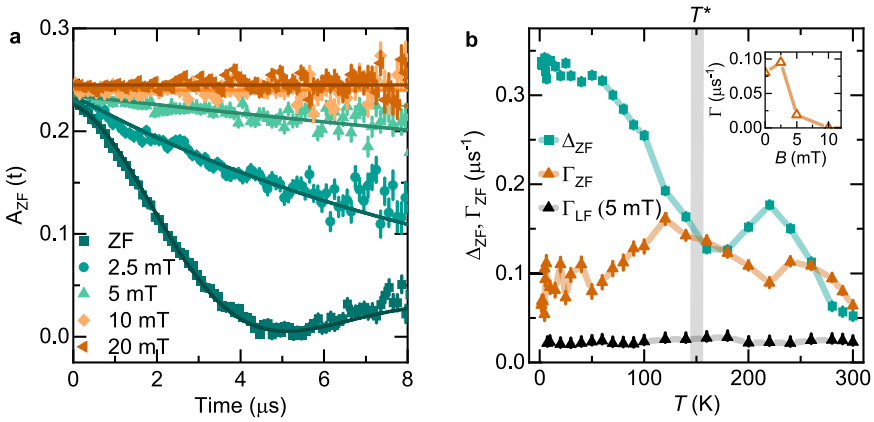

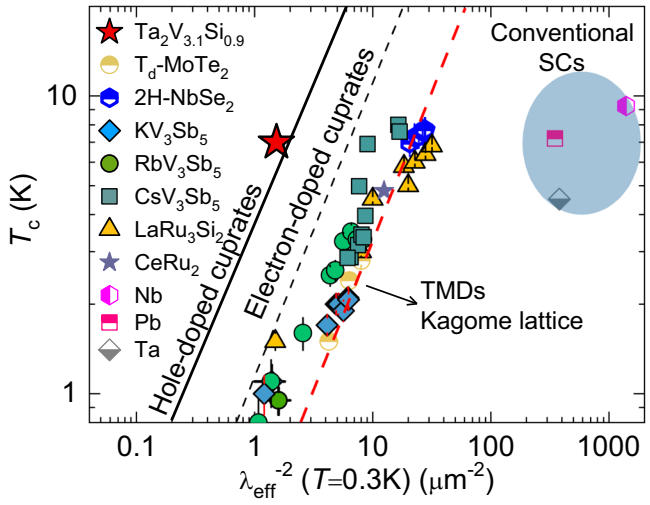

Fig. 5 | Critical temperature versus superfluid density. Plot of T_c versus $\lambda_{eff}^{-2}(0)$ on a logarithmic scale obtained from μSR experiments for the kagome-lattice superconductors KV_3Sb_5[13,35], RbV_3Sb_5[13], CsV_3Sb_5[34], $LaRu_3Si_2$[25] and $CeRu_2$[38]. The dashed red line represents the relationship obtained for the layered transition metal dichalcogenide superconductors T_d-$MoTe_2$ and 2H-$NbSe_2$ by Guguchia et al.[48,49]. The relationship observed for cuprates is also shown[50,51] as well as the points for various conventional superconductors. Modified from Ref. 20.

V_3Sb_5 = 0.45K/μm^{-2}[13,35], CsV_3Sb_5 = 0.7K/μm^{-2}[34], $LaRu_3Si_2$[25] and $CeRu_2$[38] ~ 0.37K/μm^{-2} included in Fig. 5. The ratio for $Ta_2V_{3.1}Si_{0.9}$ is T_C/λ_{eff}^2 = 4.78 K/μm^{-2}, significantly larger than the other kagome superconductors, and actually comparable to hole-doped cuprates, which are known to be correlated superconductors. The similarity in T_C/λ_{eff}^2 between $Ta_2V_{3.1}Si_{0.9}$ and the hole-doped cuprates suggests that some of the same correlation effects may be present in $Ta_2V_{3.1}Si_{0.9}$.

Additionally, the observation of low superconducting carrier density is intriguing, as it suggests that fluctuations, both classical and quantum, play a significant role in the superconducting phase[39]. Consequently, the transition to the superconducting state in these materials may deviate from typical mean-field behaviour, which in turn influence the low-temperature properties. To gain further insight into this aspect, a single-crystal study is required.

(3) The observation of the paramagnetic shift in the superconducting state of $Ta_2V_{3.1}Si_{0.9}$, instead of the expected diamagnetic shift imposed by the superconducting state. In general, the paramagnetic shift can have a few possible causes, including field induced magnetism[40,41], vortex disorder[42], an odd-superconducting pairing[43], the suppression of the negative Knight shift below T_C due to singlet pairing or the presence of paramagnetic regions in the sample[44]. The superconducting part of the sample would expel the field, resulting in an effective increase in the neighbouring paramagnetic regions. Additional experiments are needed to explore the origin of the paramagnetic shift in $Ta_2V_{3.1}Si_{0.9}$, however it is worth noting that similar behaviour was observed in the topological compound, $Nb_{0.25}Bi_2Se_3$[44].

(4) Finally, the zero-field muon spin relaxation rate of static origin increases below 150K. This enhancement of the internal field width points to a TRS breaking state below 150K, similar to the TRS breaking observed in various other kagome systems such as AV_3Sb_5[13,34–36], ScV_6Sn_6[45,46], $LaRu_3Si_2$[25] and $CeRu_2$[37,38]. Notably, in systems such as AV_3Sb_5, ScV_6Sn_6 and $LaRu_3Si_2$, the TRS breaking coincides with the onset of charge order. Conversely, in $CeRu_2$, the magnetic response occurs without charge order. This raises fundamental questions about the origin of TRS breaking in $Ta_2V_{3.1}Si_{0.9}$–is charge order involved, or does the high-temperature TRS breaking stem from a different mechanism, such as a weak spin-density wave phase without involvement of charge order? Notably, 150K would represent the highest TRS breaking temperature amongst kagome materials in the bulk, however the precise origin of this state has to be determined.

Conclusion

In conclusion, our results classify $Ta_2V_{3.1}Si_{0.9}$ as an unconventional bulk superconductor with several unusual characteristics, such as the paramagnetic shift and high-temperature transition, T^*. This observed T^* transition necessitates further investigation for which we recommend X-ray diffraction measurements to determine if it originates from charge order or has a magnetic origin without involvement of charge order. In general, we hope these results will help to elucidate the broader principles that govern superconductivity in kagome lattices and inspire further research into this promising area.

Methods

μSR experiment

A μSR (muon spin rotation) experiment involves implanting a nearly 100% spin polarised beam of muons, μ^+ into the sample one by one. Once implanted, these positively charged μ^+ particles then thermally stabilise at interstitial lattice sites, effectively acting as magnetic microprobes in an experiment. If the material is magnetic, then each muon will precess in a local field, B_{int} at the muon site with a Larmor frequency, $\upsilon_{int} = \gamma_\mu/(2\pi)B_{int}$, where the gyromagnetic ratio of the muon is defined as $\gamma_\mu/(2\pi)$ = 135.5MHz/T. The μSR technique can unveil important length scales in superconductors such as the magnetic penetration depth, λ and coherence length, ξ.

Experimental details

Zero-field (ZF), transverse-field (TF) and longitudinal-field (LF) μSR experiments at ambient pressure on the polycrystalline samples of $Ta_2V_{3.1}Si_{0.9}$ were performed on the GPS instrument (1.6–300K) and Dolly instrument (0.27–10K) at the Swiss Muon Source (SμS) at the Paul Scherrer Institute (Villigen, Switzerland). Fits of ZF μSR data were performed by both single-histogram (SH) and asymmetry (Asy) methods. In a SH fit, the background and data from each detector is individually fit, whereas in an Asy fit, since the difference between the detectors is taken, any background information is lost[47]. For materials producing a small signal, the loss of background information can distort the extracted parameters, and therefore a SH fit is more reflective of the sample.

Data availability

All relevant data are available from the authors. Alternatively, the data can be accessed through the data base at the following link http://musruser.psi.ch/cgi-bin/SearchDB.cgi using the following details: 1. Area: Dolly. Year: 2023. Run Title: 0676-0725. 2. Area: GPS. Year: 2023. Run Title: 0965-1073.

Received: 27 May 2024; Accepted: 1 October 2024;
Published online: 12 October 2024

References

1. Syôzi, I. Statistics of Kagomé Lattice. *Prog. Theor. Phys.* **6**, 306–308 (1951).
2. Yin, J.-X., Lian, B. & Hasan, M. Z. Topological kagome magnets and superconductors. *Nature* **612**, 647–657 (2022).
3. Guguchia, Z. et al. Tunable anomalous hall conductivity through volume-wise magnetic competition in a topological kagome magnet. *Nat. Commun.* **11**, 559 (2020).
4. Kiesel, M. L. & Thomale, R. Sublattice interference in the Kagome Hubbard model. *Phys. Rev. B* **86**, 121105 (2012).
5. Yang, J. et al. Observation of flat band, Dirac nodal lines and topological surface states in kagome superconductor csti3bi5. *Nat. Commun.* **14**, 4089 (2023).
6. Luo, Y. et al. A unique van Hove singularity in kagome superconductor $CsV_{3-x}Ta_xSb_5$ with enhanced superconductivity. *Nat. Commun.* **14**, 3819 (2023).
7. Kang, M. et al. Twofold van Hove singularity and origin of charge order in topological kagome superconductor CsV_3Sb_5. *Nat. Phys.* **18**, 301–308 (2022).
8. Hu, Y. et al. Rich nature of van Hove singularities in kagome superconductor CsV_3Sb_5. *Nat. Commun.* **13**, 2220 (2022).

9. Li, M. et al. Dirac cone, flat band and saddle point in kagome magnet ymn6sn6. *Nat. Commun.* **12**, 3129 (2021).
10. Ortiz, B. R. et al. CsV_3Sb_5: A $\mathbb{Z}_2$ topological kagome metal with a superconducting ground state. *Phys. Rev. Lett.* **125**, 247002 (2020).
11. Ortiz, B. R. et al. Superconductivity in the $\mathbb{Z}_2$ kagome metal KV_3Sb_5. *Phys. Rev. Mater.* **5**, 034801 (2021).
12. Yin, Q. et al. Superconductivity and normal-state properties of kagome metal RbV_3Sb_5 single crystals. *Chin. Phys. Lett.* **38**, 037403 (2021).
13. Guguchia, Z. et al. Tunable unconventional kagome superconductivity in charge ordered RbV_3Sb_5 and KV_3Sb_5. *Nat. Commun.* **14**, 153 (2023).
14. Yu, F. et al. Pressure-induced dimensional crossover in a kagome superconductor. *Phys. Rev. Lett.* **128**, 077001 (2022).
15. LaBollita, H. & Botana, A. S. Tuning the van Hove singularities in AV_3Sb_5(A = K, Rb, Cs) via pressure and doping. *Phys. Rev. B* **104**, 205129 (2021).
16. Zhang, Z. et al. Pressure-induced reemergence of superconductivity in the topological kagome metal CsV_3Sb_5. *Phys. Rev. B* **103**, 224513 (2021).
17. Graham, J. N. et al. Depth-dependent study of time-reversal symmetry-breaking in the kagome superconductor AV_3Sb_5. Preprint at https://doi.org/10.48550/arXiv.2402.11130 (2024).
18. Yang, S.-Y. et al. Giant, unconventional anomalous hall effect in the metallic frustrated magnet candidate, KV_3Sb_5. *Sci. Adv.* **6**, eabb6003 (2020).
19. Jiang, Y.-X. et al. Unconventional chiral charge order in kagome superconductor KV_3Sb_5. *Nat. Mater.* **20**, 1353–1357 (2021).
20. Guguchia, Z., Khasanov, R. & Luetkens, H. Unconventional charge order and superconductivity in kagome-lattice systems as seen by muon-spin rotation. *NPJ Quantum Mater.* **8**, 41 (2023).
21. Vandenberg, J. & Barz, H. The crystal structure of a new ternary silicide in the system rare-earth-ruthenium-silicon. *Mater. Res. Bull.* **15**, 1493–1498 (1980).
22. Kishimoto, Y. et al. Magnetic susceptibility study of $LaRu_3Si_2$. *J. Phys. Soc. Jpn.* **71**, 2035–2038 (2002).
23. Li, B., Li, S. & Wen, H.-H. Chemical doping effect in the $LaRu_3Si_2$ superconductor with a kagome lattice. *Phys. Rev. B* **94**, 094523 (2016).
24. Li, S. et al. Anomalous properties in the normal and superconducting states of $LaRu_3Si_2$. *Phys. Rev. B* **84**, 214527 (2011).
25. Mielke III, C. et al. Nodeless kagome superconductivity in $LaRu_3Si_2$. *Phys. Rev. Mater.* **5**, 034803 (2021).
26. Mielke III, C. et al. Charge orders with distinct magnetic response in a prototypical kagome superconductor $LaRu_3Si_2$. Preprint at https://doi.org/10.48550/arXiv.2402.16219 (2024).
27. Liu, H. et al. Vanadium-based superconductivity in the breathing kagome compound $Ta_2V_{3.1}Si_{0.9}$. *Phys. Rev. B* **108**, 104504 (2023).
28. Suter, A. & Wojek, B. Musrfit: A free platform-independent framework for μsr data analysis. *Phys. Procedia* **30**, 69–73 (2012).
29. Brandt, E. H. Flux distribution and penetration depth measured by muon spin rotation in high-T_c superconductors. *Phys. Rev. B* **37**, 2349–2352 (1988).
30. Brandt, E. H. Properties of the ideal ginzburg-landau vortex lattice. *Phys. Rev. B* **68**, 054506 (2003).
31. Carrington, A. & Manzano, F. Magnetic penetration depth of MgB_2. *Phys. C Supercond.* **385**, 205–214 (2003).
32. Fang, M. H. et al. Superconductivity close to magnetic instability in $Fe(Se_{1-x}Te_x)_{0.82}$. *Phys. Rev. B* **78**, 224503 (2008).
33. Li, H. et al. Rotation symmetry breaking in the normal state of a kagome superconductor KV_3Sb_5. *Nat. Phys.* **18**, 265–270 (2022).
34. Gupta, R. et al. Microscopic evidence for anisotropic multigap superconductivity in the CsV_3Sb_5 kagome superconductor. *NPJ Quantum Mater.* **7**, 49 (2022).
35. Mielke III, C. et al. Time-reversal symmetry-breaking charge order in a kagome superconductor. *Nature* **602**, 245–250 (2022).
36. Khasanov, R. et al. Time-reversal symmetry broken by charge order in CsV_3Sb_5. *Phys. Rev. Res.* **4**, 023244 (2022).
37. Deng, L. et al. Effect of fermi surface topology change on the kagome superconductor $CeRu_2$ under pressure. *Mater. Today Phys.* **40**, 101322 (2024).
38. Mielke III, C. et al. Local spectroscopic evidence for a nodeless magnetic kagome superconductor $CeRu_2$. *J. Phys. Condens. Matter* **34**, 485601 (2022).
39. Emery, V. & Kivelson, S. Importance of phase fluctuations in superconductors with small superfluid density. *Nature* **374**, 434–437 (1995).
40. Khasanov, R. et al. Superconductivity and field-induced magnetism in $SrFe_{1.75}Co_{0.25}As_2$. *Phys. Rev. Lett.* **103**, 067010 (2009).
41. Guguchia, Z. et al. Probing the pairing symmetry in the over-doped fe-based superconductor $Ba_{0.35}Rb_{0.65}Fe_2As_2$ as a function of hydrostatic pressure. *Phys. Rev. B* **93**, 094513 (2016).
42. Sonier, J. E. et al. Magnetism and disorder effects on muon spin rotation measurements of the magnetic penetration depth in iron-arsenic superconductors. *Phys. Rev. Lett.* **106**, 127002 (2011).
43. Krieger, J. A. et al. Proximity-induced odd-frequency superconductivity in a topological insulator. *Phys. Rev. Lett.* **125**, 026802 (2020).
44. Das, D. et al. Time-reversal invariant and fully gapped unconventional superconducting state in the bulk of the topological compound $Nb_{0.25}Bi_2Se_3$. *Phys. Rev. B* **102**, 134514 (2020).
45. Guguchia, Z. et al. Hidden magnetism uncovered in a charge ordered bilayer kagome material ScV_6Sn_6. *Nat. Commun.* **14**, 7796 (2023).
46. Yi, C., Feng, X., Kumar, N., Felser, C. & Shekhar, C. Tuning charge density wave of kagome metal ScV_6Sn_6. Preprint at https://doi.org/10.48550/arXiv.2403.02463 (2024).
47. Amato, A. & Morenzoni, E. *Introduction to Muon Spin Spectroscopy: Applications to Solid State and Material Sciences*. Lecture Notes in Physics (Springer International Publishing, 2024). https://books.google.ch/books?id=d4Qa0AEACAAJ
48. Von Rohr, F. et al. Unconventional scaling of the superfluid density with the critical temperature in transition metal dichalcogenides. *Sci. Adv.* **5**, eaav8465 (2019).
49. Guguchia, Z. et al. Signatures of the topological s+- superconducting order parameter in the type-ii weyl semimetal T_d-$MoTe_2$. *Nat. Commun.* **8**, 1082 (2017).
50. Uemura, Y. et al. Universal correlations between T_c and n_s/m^*(carrier density over effective mass) in high-T_c cuprate superconductors. *Phys. Rev. Lett.* **62**, 2317 (1989).
51. Shengelaya, A. et al. Muon-spin-rotation measurements of the penetration depth of the infinite-layer electron-doped $Sr_{0.9}La_{0.1}CuO_2$ cuprate superconductor. *Phys. Rev. Lett.* **94**, 127001 (2005).

Acknowledgements

The muon spectroscopy studies were performed at the Swiss Muon Source (SμS) Paul Scherrer Insitute, Villigen, Switzerland. Z.G. acknowledges support from the Swiss National Science Foundation (SNSF) through SNSF Starting Grant (No. TMSGI2_211750). Z.G. acknowledges discussions with Prof. Stephan Wilson and with Dr. Robert Johann Scheuermann. The Natural Science Foundation of China (Grant Grants No. U2032204, U22A6005), and the Synergetic Extreme Condition User Facility (SECUF).

Author contributions

Z.G. conceived and supervised the project. Growth of the polycrystalline samples $Ta_2V_{3.1}Si_{0.9}$: H.Liu, and Y.S. Magnetisation experiments: J.N.G, M.M. and Z.G. Muon spin rotation experiments, analysis and corresponding discussions: J.N.G, V.S., C.M.III, H.L., R.K., and Z.G. Figure development and writing of the paper: J.N.G and Z.G. All authors discussed the results, interpretation and conclusion.

Competing interests

The authors declare no competing interests.

Additional information

Supplementary information The online version contains supplementary material available at https://doi.org/10.1038/s43246-024-00666-2.

Correspondence and requests for materials should be addressed to Z. Guguchia.

Peer review information *Communications Materials* thanks the anonymous reviewers for their contribution to the peer review of this work. Primary Handling Editors: Toru Hirahara and Aldo Isidori. A peer review file is available.